LANGMUIR Article
Cite This: *Langmuir* 2019, 35, 15063−15070 pubs.acs.org/Langmuir

Characterizing the Supported Lipid Membrane Formation from Cholesterol-Rich Bicelles

Tun Naw Sut,[†] Soohyun Park,[†] Younghwan Choe,[‡] and Nam-Joon Cho*[,†]

[†]School of Materials Science and Engineering, Nanyang Technological University, 50 Nanyang Avenue, 639798, Singapore
[‡]Department of Chemistry, Columbia University, 3000 Broadway, New York 10027, United States

Supporting Information

ABSTRACT: Supported lipid bilayers (SLBs) are simplified model membrane systems that mimic the fundamental properties of biological cell membranes and allow the surface-sensitive tools to be used in numerous sensing applications. SLBs can be prepared by various methods including vesicle fusion, solvent-assisted lipid bilayer (SALB), and bicelle adsorption and are generally composed of phospholipids. Incorporating other biologically relevant molecules, such as cholesterol (Chol), into SLBs has been reported with the vesicle fusion and SALB methods, whereas it remains unexplored with the bicelle absorption method. Herein, using the quartz crystal microbalance-dissipation (QCM-D) and fluorescence microscopy techniques, we explored the possibility of forming SLBs from Chol-containing bicelles and discovered that Chol-enriched SLBs can be fabricated with bicelles. We also compared the Chol-enriched SLB formation of the bicelle method to that of vesicle fusion and SALB and discussed how the differences in lipid assembly properties can cause the differences in the adsorption kinetics and final results of SLB formation. Collectively, our findings demonstrate that the vesicle fusion method is least favorable for forming Chol-enriched SLBs, whereas the SALB and bicelle methods are more favorable, highlighting the need to consider the application requirements when choosing a suitable method for the formation of Chol-enriched SLBs.

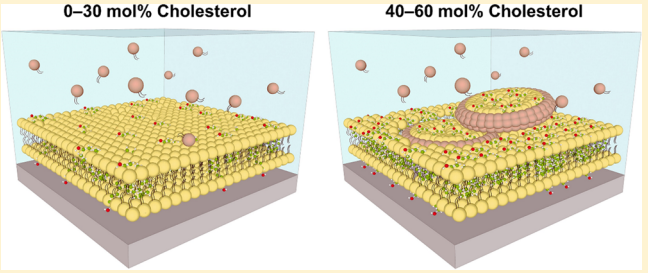

INTRODUCTION

Cholesterol (Chol) is an important component in biological membranes that is required for normal cell functions.[1] It regulates the membrane rigidity, permeability, and protein interactions and plays a role in membrane remodeling.[1−5] However, if present in a high amount, it can affect cells negatively and cause them to be in various diseased states.[6,7] Therefore, understanding how Chol influences the membrane properties and behaviors is essential. To do so, artificial lipid membrane models that mimic the fundamental architecture of natural cell membranes have been developed and proven useful.[8] Their composition can be controlled and simplified to include just one or a few components,[9−11] and this makes it easier to study the specific effects/events related to those components. Among the several model membrane systems, supported lipid bilayers (SLBs) that are formed on solid surfaces have advantage of enabling the use of surface-sensitive analytical tools in biophysical studies of membranes as well as in sensing applications.[12]

There are numerous methods to fabricate SLBs, and at present, the vesicle fusion method is the most widely used method. It involves the adsorption and rupture of lipid vesicles on solid supports.[13] Various experimental parameters including vesicle composition can affect SLB formation by vesicle fusion.[14] In particular, the high Chol content has been shown to hinder vesicle rupture,[15] and the preparation of complete, homogeneous SLBs is therefore challenging in the vesicle fusion method. Recently, our group has reported successful fabrication of Chol-rich SLBs via an alternative method called the solvent-assisted lipid bilayer (SALB).[16,17] The method involves the deposition of lipids dissolved in an organic solvent (e.g., isopropanol) onto a solid support, followed by aqueous solvent exchange that induces phase transitions, leading to SLB formation on the support.[18−21] We have shown that SLBs containing up to around 60 mol % Chol can be prepared by the SALB whereas SLBs formed by the vesicle fusion contain only up to 10 mol % Chol.[16,17] Despite its ability to fabricate Chol-rich SLBs, the SALB method limits the direct formation of SLBs in aqueous solutions, as the deposition of lipids in organic solvents precedes the exchange to aqueous solution.

To this end, one promising method involves the adsorption of bicelles in aqueous solution. Bicelles are mixtures of long-chain and short-chain phospholipids[22,23] and typically considered as two-dimensional disks that have been extensively used in structural biology studies.[24,25] Zeineldin et al. first demonstrated SLB formation from lipid bicelles composed of long-chain 1,2-dipalmitoyl-*sn*-glycero-3-phosphocholine

Received: September 10, 2019
Revised: October 31, 2019
Published: October 31, 2019

DOI: 10.1021/acs.langmuir.9b02851
Langmuir 2019, 35, 15063−15070

(DPPC) and short-chain 1,2-diheptanoyl-*sn*-glycero-3-phosphocholine ($DHPC_7$) lipids.[26] Following works by Tabaei et al.[27] and Morigaki et al.[28] used bicelles composed of long-chain dimyristoylphosphatidylcholine (DMPC) and 1-palmitoyl-2-oleol-*sn*-glycero-3-phosphocholine (POPC) lipids, respectively, and short-chain 1,2-dihexanoyl-*sn*-glycero-3-phosphocholine ($DHPC_6$, referred to as DHPC in the following text) lipids. More recently, our group has reported bicelle works using a different long-chain 1,2-dioleoyl-*sn*-glycero-3-phosphocholine (DOPC), either alone[29,30] or in combination with other charged long-chain lipids such as 1,2-dioleoyl-*sn*-glycero-3-ethylphosphocholine (DOEPC) and 1,2-dioleoyl-*sn*-glycero-3-phospho-L-serine (DOPS).[31] The possibility of forming SLBs with Chol-containing bicelles therefore remains to be explored.

Here, we investigated the adsorption behavior of cholesterol-rich bicelles and corresponding SLB formation capability on silicon dioxide surfaces. Quartz crystal microbalance-dissipation (QCM-D) and fluorescence microscopy experiments including fluorescence recovery after photobleaching (FRAP) measurements were conducted to characterize SLB formation and properties, as outlined in Figure 1. The results were also

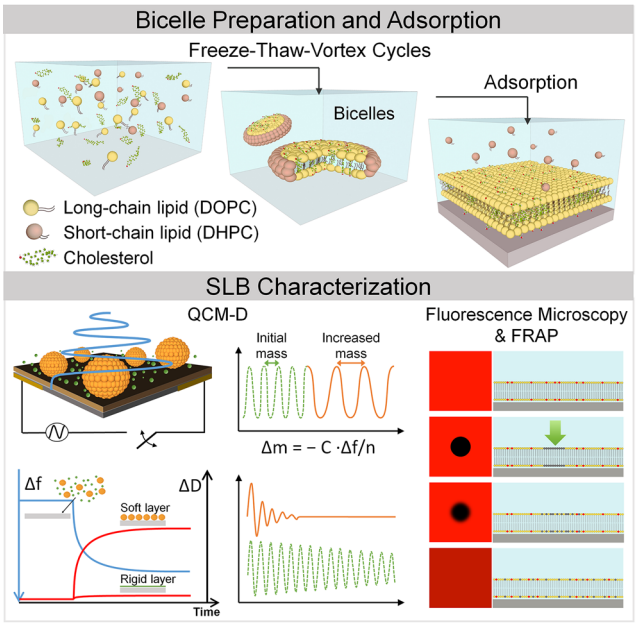

Figure 1. Overview of experimental strategy. The cholesterol-containing bicelles were prepared by simple freeze–thaw–vortex cycles. Bicelle adsorption onto silicon dioxide surfaces and membrane properties were characterized by QCM-D and fluorescence microscopy.

compared to our previous data obtained with vesicle fusion and SALB methods[16,17] using Chol-containing lipids. Our findings demonstrate that Chol-rich SLBs can be formed via the bicelle method and they have different properties than those formed via the other two methods.

MATERIALS AND METHODS

Reagents. 1,2-Dioleoyl-*sn*-glycero-3-phosphocholine (DOPC), 1,2-dihexanoyl-*sn*-glycero-3-phosphocholine (DHPC), and 1,2-dioleoyl-*sn*-glycero-3-phosphoethanolamine-*N*-(lissamine rhodamine B sulfonyl) (ammonium salt) (red, Rh-PE) lipids dispersed in chloroform, and cholesterol (Chol) powder were obtained from Avanti Polar Lipids (Alabaster, AL, USA). The excitation/emission wavelengths of Rh-PE were 560/583 nm. Methyl-β-cyclodextrin (MβCD) was purchased from Sigma-Aldrich (Singapore). The buffer used in all experiments was 10 mM Tris buffer with 150 mM NaCl (pH 7.5). Buffers and solutions were prepared with Milli-Q-treated water (MilliporeSigma, Burlington, MA, USA).

Bicelle Preparation. Bicelles were prepared by lipid hydration followed by the freeze–thaw–vortex step, as previously described.[29] Briefly, the cholesterol powder was dissolved in chloroform and mixed with long-chain DOPC phospholipids in a glass vial. Then, the chloroform solvent was evaporated with nitrogen gas, forming a dry lipid film on the walls of the glass vial. The lipid film was then stored overnight in a vacuum desiccator to remove trace residues of chloroform, followed by subsequent hydration in a DHPC-containing aqueous buffer solution comprising 10 mM Tris (pH 7.5) and 150 mM NaCl. The resulting lipid suspension had a long-chain phospholipid concentration of 1 mM and a q-ratio of 0.25. The lipid suspensions were then subjected to five freeze–thaw–vortex cycles that involved the following steps: submersion in liquid nitrogen for 1 min, thawing in a 60 °C water bath for 5 min, and vortexing for 30 s. The resulting suspensions were visually clear at room temperature. Immediately before the experiment, an aliquot of the stock lipid suspension was diluted ~32-fold by using the buffer solution so that the final long-chain phospholipid concentration was 0.031 mM.

Quartz Crystal Microbalance-Dissipation (QCM-D). Bicelle adsorption experiments were conducted using a Q-Sense E4 instrument (Biolin Scientific AB, Stockholm, Sweden). The quartz crystal sensors were repeatedly rinsed with water and ethanol, dried with nitrogen gas, and then treated in an oxygen plasma chamber (PDC-002, Harrick Plasma, Ithaca, NY) for 1 min. The temperature of the QCM-D chambers was maintained at 25 °C. All solutions were added under continuous flow conditions using a peristaltic pump (Reglo Digital MS-4/6, Ismatec, Wertheim, Germany), and the flow rate was set at 50 μL/min. Measurement data were collected at multiple odd overtones by the Q-Soft software package (Biolin Scientific AB). The reported data were collected at the 7th overtone and normalized according to the overtone number. Data processing was completed using the Q-Tools (Biolin Scientific AB) and OriginPro (OriginLab, Northampton, MA) software programs.

Epifluorescence Microscopy. Imaging experiments were conducted using a Nikon Eclipse Ti-E inverted microscope with a 60× oil-immersion objective (NA 1.49). The excitation source was a mercury-fiber illuminator C-HGFIE Intensilight (Nikon, Tokyo, Japan), and the light was passed through a TRITC filter block (Ex 545/30, Em 605/70) for imaging red channels. An Andor iXon3 897 EMCCD camera was used to obtain the images at the rate of 1 frame per 3 s. The experiments were conducted within a flow-through, microfluidic chamber (sticky-Slide VI 0.4, ibidi GmbH, Martinsried, Germany), and the liquid sample was introduced at a flow rate of 50 μL/min, as controlled by a peristaltic pump (Reglo Digital MS-4/6). All measurements were conducted at room temperature (~25 °C).

RESULTS AND DISCUSSION

Quartz Crystal Microbalance-Dissipation. We performed QCM-D experiments to monitor the self-assembly of cholesterol-rich bicelles and subsequent formation of supported lipid membranes on silicon dioxide surfaces. The shifts in frequency (Δf) and energy dissipation (ΔD) of silicon dioxide-coated piezoelectric quartz crystals due to bicelle adsorption were recorded as a function of time. Δf reflects the mass changes, and ΔD relates to the viscoelastic properties of adsorbed lipid molecules.[32] In the experiments, a baseline signal in aqueous buffer solution was first obtained before bicelles were added and flowed continuously until the Δf and ΔD values stabilized. Then, a buffer washing step was performed to remove nonadsorbed or weakly adsorbed lipids, and the final Δf and ΔD shifts were recorded for each measurement run (n = 3). The q-ratio of 0.25 and long-chain

DOI: 10.1021/acs.langmuir.9b02851
Langmuir 2019, 35, 15063−15070

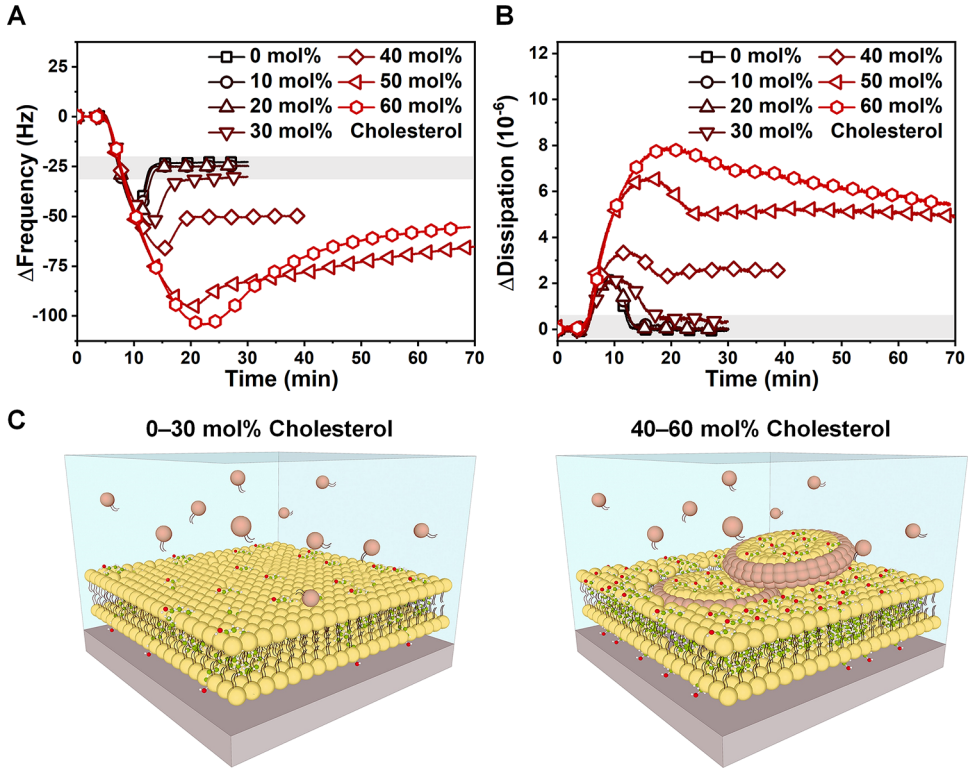

Figure 2. QCM-D measurements of adsorption of cholesterol-containing bicelles onto silicon dioxide. The data are presented for changes in (A) frequency and (B) energy dissipation as a function of time for the adsorption cases of bicelles containing different molar ratios of cholesterol. Baseline signals in equivalent buffer solution were recorded before injecting bicelles at 5 min. The grey shade denotes typical values of a complete SLB. (C) Schematic representations of the supported lipid membranes: complete SLB (left) and incomplete SLB (right).

lipid concentration of 0.031 mM were chosen based on our previous study where the optimal conditions were identified for SLB formation from DOPC/DHPC bicellar mixtures.[29] The molar fraction (mol %) of Chol in bicelles was varied from 0 to 60 mol % in 10 mol % increments with respect to that of long-chain DOPC lipids, while DHPC lipid amount was fixed. The QCM-D kinetics of all bicelle adsorption cases is presented in Figure 2A for the Δf shifts and Figure 2B for the corresponding ΔD shifts.

Adsorption of DOPC/DHPC bicelles (0 mol % Chol) led to the final Δf and ΔD shifts around -25.1 ± 2.6 Hz and $0.1 \pm 0.1 \times 10^{-6}$, respectively, which are consistent with complete SLB formation,[33] as expected. Similarly, complete SLBs resulted from the adsorption of bicelles containing 10 and 20 mol % Chol. The final Δf and ΔD shifts for the 10 mol % Chol case were around -25.5 ± 0.7 Hz and $0.1 \pm 0.2 \times 10^{-6}$, respectively, and for the 20 mol % Chol case, around -25.1 ± 0.6 Hz and $0.0 \pm 0.1 \times 10^{-6}$, respectively. For the 30 mol % Chol case, there was a final Δf of around -31.0 ± 1.0 Hz and ΔD of around $0.4 \pm 0.2 \times 10^{-6}$. The Δf value was slightly higher than the Δf range for an SLB, suggesting the presence of either unruptured bicelles or additional mass, whereas the ΔD shift was within the SLB range, indicating complete rupture and formation of a rigid layer. Taken together, the possibility of the presence of unruptured bicelles can be ruled out, and the slight increase in Δf can be attributed to additional mass as a result of rigid Chol molecules filling the interstitial spaces between lipids and causing the lipids to pack more closely[8,34] (i.e., tighter packing density) without viscoelastic contribution. Thus, we can conclude that SLB formation is complete in this case.

By marked contrast, when the molar fraction of Chol was further increased to 40 mol %, the final Δf and ΔD shifts resulted in -52.0 ± 2.8 Hz and $2.5 \pm 0.2 \times 10^{-6}$, respectively. These values are higher than SLBs, indicating incomplete bicelle rupture. Similar results with greater kinetic shifts were obtained at 50 mol % Chol, and the final Δf and ΔD values reached around -68.0 ± 2.4 Hz and $5.1 \pm 0.1 \times 10^{-6}$, respectively, suggesting bicelle rupture is even less favorable, as expected. At 60 mol % Chol, the final Δf and ΔD were around -56.0 ± 3.7 Hz and $5.5 \pm 0.2 \times 10^{-6}$, respectively, which also indicate incomplete bicelle rupture. Interestingly, the final Δf was smaller than that at 50 mol % Chol, and the reason could be the greater bicelle deformation and/or higher degree of bicelle rupture due to more water mass released. However, it is unlikely because the ΔD shifts were similar, suggesting rather equal water mass contribution and hence similar degree of rupture. Moreover, the fact that Chol hinders complete rupture of lipid vesicles by reducing lipid–lipid interaction[15] can hold true for lipid bicelles, which also need to undergo complete rupture to form SLB. Therefore, another aspect left to consider is the lipid mass contribution, and for this, the following two factors can be taken into account: (1) Chol at 60 mol % is close to its solubility limit in phosphatidylcholine (PC) bilayers,[35] and Chol bilayer domains (CBDs) where Chol molecules assemble into a bilayer-like structure within Chol-saturated PC bilayers start to form;[36] and (2) the local length of CBDs is shorter than the length of the surrounding PC bilayer patches, which could be either the flat regions of unruptured lipid bicelles or the formed SLB areas. Taken together, we can derive that the local thickness reduction in the CBDs at 60 mol % Chol caused a decrease in the final Δf

DOI: 10.1021/acs.langmuir.9b02851
Langmuir 2019, 35, 15063−15070

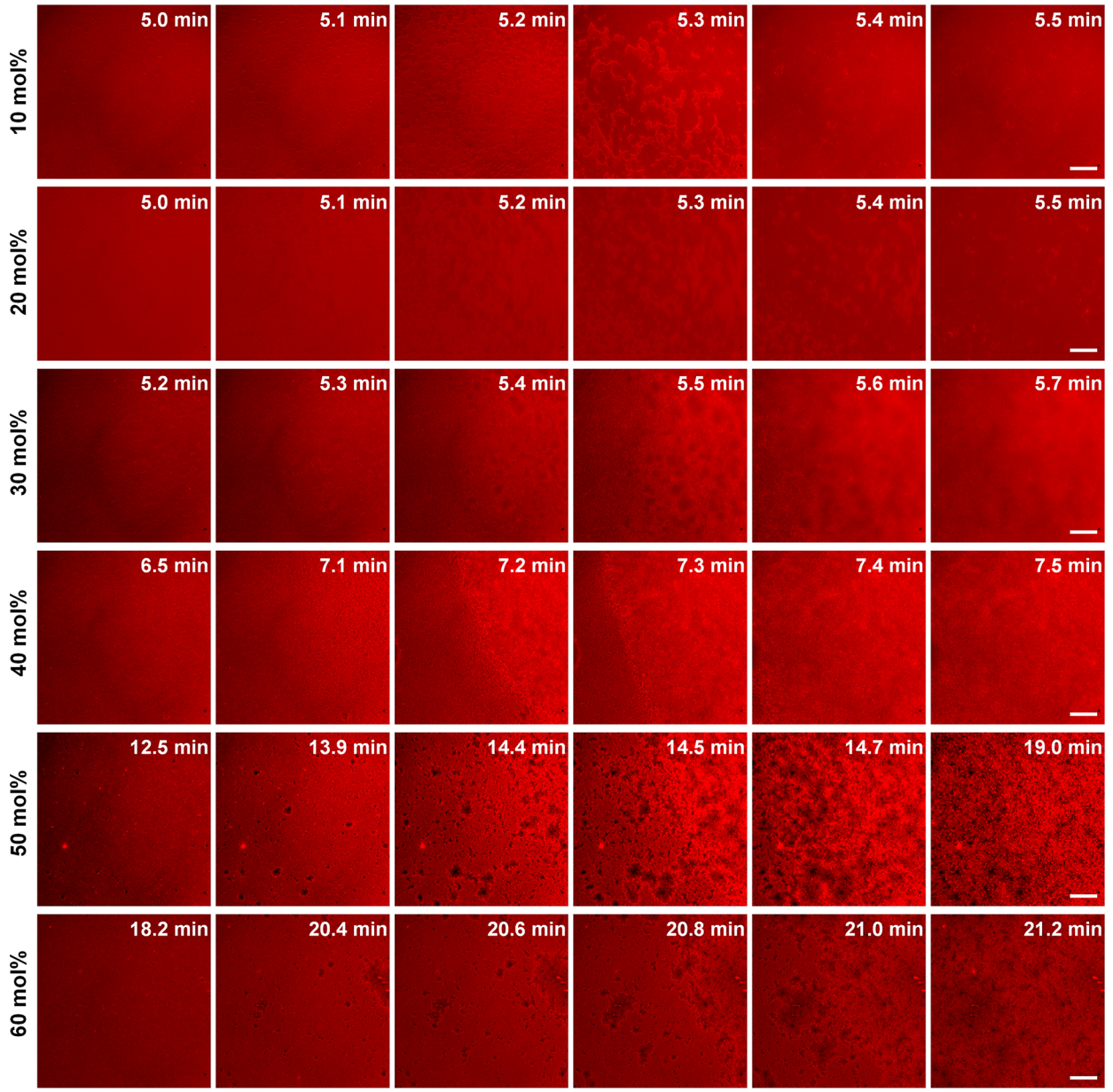

Figure 3. Direct observation of the supported lipid membrane formation from cholesterol-rich bicellar mixtures. Microscopic observation of the supported lipid membrane formation on a glass surface for 10−60 mol % cholesterol-containing bicellar mixtures. Image snapshots at various time points depict the rupture of the absorbed bicelles as a part of the membrane formation process. t = 0 min corresponds to the time when bicelle addition was begun, and the time presented in the first images of the corresponding cholesterol mole fraction approximates to the time when the critical bicelle coverage was reached. The scale bars are 20 μm.

without affecting the global viscoelasticity of the lipid membrane.

In all cases, the bicelle adsorption followed a two-step pathway in which bicelles adsorb until a critical surface coverage is reached and then rupture fully for complete SLB formation or partially for incomplete SLB formation. Overall, the results show that complete SLB formation can be achieved with a Chol fraction up to 30 mol % and incomplete SLB formation with 40−60 mol % Chol where some bicelles remain intact in the membrane.

Epifluorescence Microscopy. In addition to QCM-D characterization, we performed epifluorescence microscopy experiments to visually observe the bicelle adsorption and supported lipid membrane formation processes. The bicelles were labelled with 0.5 mol % (with respect to DOPC mole percent) of Rh-PE fluorescent lipids for imaging purposes and then added into a microfluidic chamber under flow-through conditions for capturing time-lapsed images. The initial injection time was defined as t = 0 min, and the time shown in the first images corresponds to the time when the adsorbed bicelles reached the critical coverage on the surface. The results are presented in Figure 3 and explained below.

Bicelles with 10 and 20 mol % Chol adsorbed rapidly and reached the critical surface coverage after around 5 min. Then, the bicelle fusion as indicated by the appearance of small bright spots and subsequent SLB formation with uniform fluorescence properties followed quickly in 0.5 min. With 30 mol % Chol, the critical coverage was reached after around 5.2 min and bilayer propagation occurred within 0.5 min also. As the Chol fraction increased further, it took longer time to reach the

DOI: 10.1021/acs.langmuir.9b02851
Langmuir 2019, 35, 15063−15070

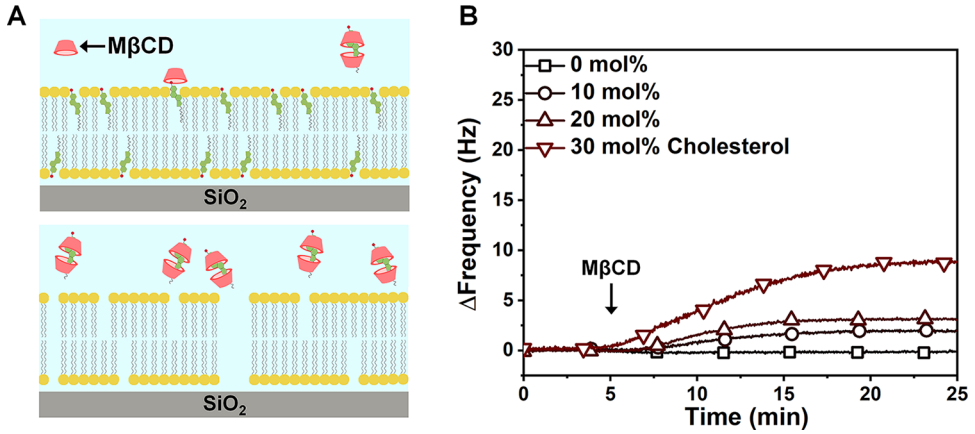

Figure 4. Quantifying the molar fraction of cholesterol in SLB. (A) Schematic representation of cholesterol extraction by MβCD. Upon adsorption of lipid mixtures and subsequent SLB formation, 1 mM MβCD was added to extract cholesterol from the SLB. (B) QCM-D frequency shifts due to MβCD treatment. The baseline frequency of 0 Hz corresponds to the normalized frequency shift before MβCD treatment.

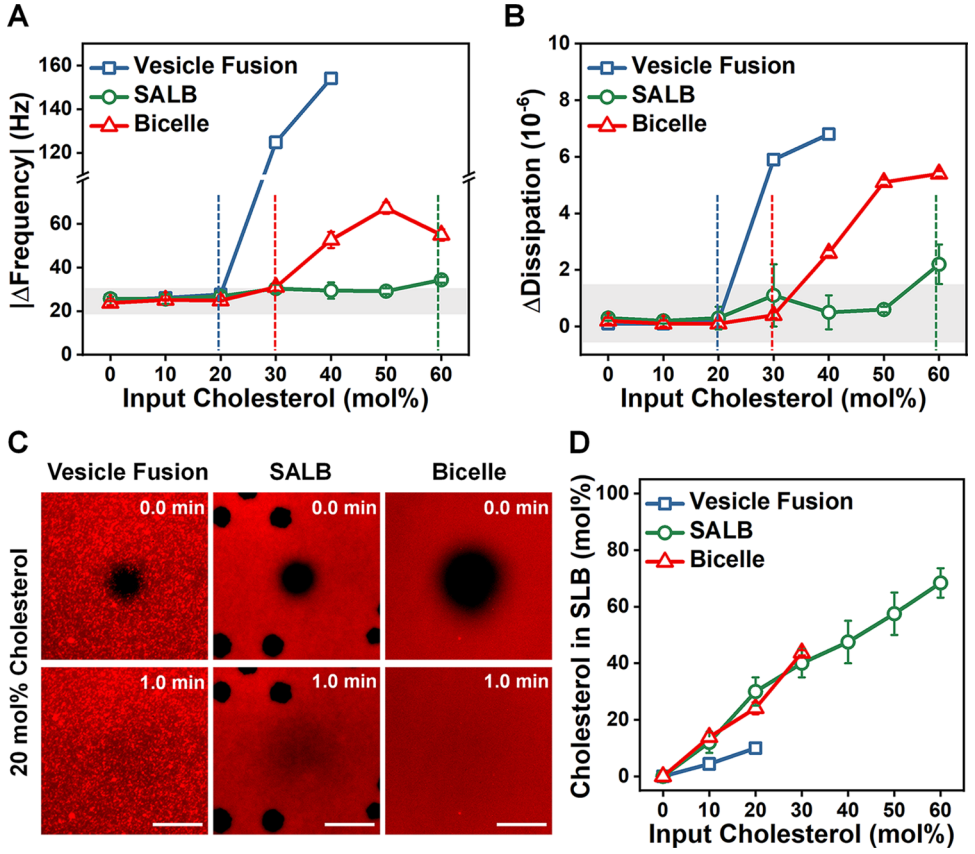

Figure 5. Data summary for SLB formation via vesicle fusion, SALB, and bicelle methods. QCM-D (A) frequency and (B) dissipation shifts. Input cholesterol refers to the mole percent of cholesterol in the precursor mixture. (C) FRAP images of SLBs formed at 20 mol % input cholesterol in each method. All scale bars are 20 μm. (D) Molar fraction of cholesterol in SLB as a function of input cholesterol fraction.

critical surface coverage (6.5 min for 40 mol %, 12.5 min for 50 mol %, and 18.2 min for 60 mol % Chol) and bilayer propagation became slower. At 40 mol % Chol, the formed lipid membrane exhibited nonuniform fluorescence properties. At 50 and 60 mol % Chol, the dark regions appeared in the membranes, indicating the presence of unlabeled Chol domains. Interestingly, unlike the QCM-D data that suggest some bicelles remain intact at 40−60 mol % Chol, there was no direct observation of unruptured bicelles in the microscopy experiments at these Chol fractions. This is different from the case of unruptured lipid vesicles, which are seen as bright dots in the membranes[30] and likely related to the difference in structure; bicelles have a two-dimensional disk-like structure,[24,37−40] whereas vesicles are in a spherical shape. The coexistence of planar disks (with flat regions of long-chain phospholipids assembled into bilayers) with SLB patches probably causes no distinction in appearance under microscopy.

We further characterized the fluidity properties of membranes by conducting FRAP experiments (Figure S1).

DOI: 10.1021/acs.langmuir.9b02851
Langmuir 2019, 35, 15063−15070

The FRAP technique reveals the mobility of lipid molecules in the membrane by determining the fluorescence recovery profile over time.[41] Briefly, upon supported lipid membrane formation, a small region in the membrane is photobleached and recovery of fluorescence is measured over time as the bleached lipids diffuse out of the region and the fluoresced lipids diffuse in from the neighboring region (Figure S1A). At 10−30 mol % Chol, fluorescence recovery was almost complete, that is, comparable to around 80% in SLB without Chol, and reduced to around 70, 65, and 60% at 40, 50, and 60 mol % Chol, respectively (Figure S1B). The reduction in mobile fractions at 40−60 mol % Chol confirms the presence of intact bicelles and agrees well with QCM-D data that show similar overall trends: complete SLB formation up to 30 mol % Chol and incomplete SLB formation with unruptured bicelles at 40−60 mol % Chol.

Quantification of Cholesterol in Supported Lipid Membranes. Next, we quantified the molar fraction of Chol in the supported lipid membranes by treating the membranes with 1 mM methyl-β-cyclodextrin (MβCD) that specifically extracts Chol from lipid membranes[42] (Figure 4A) and monitoring the kinetics of extraction with QCM-D. When 1 mM MβCD was added to the membranes, there were positive Δf shifts (Figure 4B), consistent with a decrease in the mass because of Chol extraction by MβCD. To calculate the Chol amount in the membrane, the difference between the Δf after membrane formation and the final Δf after MβCD addition was converted to mass using the Sauerbrey relationship,[43] taking the molecular weights of both DOPC and Chol into account. For the 40−60 mol % Chol cases, the Sauerbrey relationship is invalid because the membranes are not rigid as indicated by high ΔD values. Thus, we were able to calculate the Chol fraction only for the rigid membranes with low ΔD shifts (i.e., SLBs formed at 10−30 mol % Chol). The Chol mole percent in the SLBs is almost linearly proportional to that in the precursor mixtures, with a slight increase (see Figure 5D for data).

We also followed the extraction process by microscopy (Figure S2). After MβCD treatment, significant alterations in the membranes were observed. Dark regions indicative of Chol-depleted area and perturbed membrane edges appeared (Figure S2A). We estimated the total defected area % using these dark regions and related it to the Chol fraction in the membranes. There was a nearly linear relationship between the defected area % and the amount of Chol in the precursor mixture (Figure S2B), which is consistent with the QCM-D data.

SLB Formation and Cholesterol Enrichment Trends in Comparison to Vesicle Fusion and SALB. We now discuss the SLB formation and Chol enrichment of the bicelle method in comparison to those of vesicle fusion and SALB methods, which we have reported previously.[16,17] This discussion will help us understand the mechanistic differences in SLB formation among the different methods as a result of Chol addition. In short, bicelle-mediated SLB formation involves the adsorption and spontaneous rupture of lipid bicelles on solid supports as demonstrated above, which is analogous to vesicle fusion,[13] except that lipid vesicles are used instead of bicelles. The SALB method includes the deposition of lipids onto solid surfaces in an organic solvent and exchange of the solvent to aqueous solution, which brings about a series of lipid phase transitions leading to SLB formation.[19,44]

In our previous reports, we showed that the vesicle fusion can result in successful SLB formation with up to 20 mol % Chol whereas the SALB up to 60 mol % Chol.[16,17] In this study, we have demonstrated that the bicelle method can form complete SLBs with up to 30 mol % Chol and incomplete SLBs with 40−60 mol % Chol. The QCM-D and FRAP results of all three methods are reproduced and presented here for comparison (Figure 5). In terms of QCM-D results, we present the final Δf (Figure 5A) and ΔD (Figure 5B) shifts as a function of the Chol fraction to identify the maximum cutoff Chol mole percent for complete SLB formation in each method. Based on these shifts, the maximum Chol fraction that can be incorporated into SLB is 20 mol % for vesicle fusion, 60 mol % for SALB (slightly higher QCM-D shifts at 60 mol % caused by stripe superstructures[17]), and 30 mol % for the bicelle method. Note that the incomplete SLB formation by the bicelle method with 40 and 50 mol % Chol is due to the presence of Chol and with 60 mol % Chol due to the formation of CBDs.

The FRAP results are used to compare the fluidity and morphology of SLBs. In Figure 5C, we show the FRAP images obtained at 20 mol % Chol as representative SLBs formed in each method. All SLBs are fluidic, as indicated by near-complete fluorescence recovery. However, the SLB morphology in vesicle fusion is different from that in SALB, whereas it is similar to that in the bicelle method. The dark spots in SLB formed by SALB represent the Chol-rich phase in which Rh-PE lipids are excluded.[16] By contrast, there is no visible phase separation in SLBs formed by vesicle fusion and bicelle methods. Similar cases have been reported for the membranes composed of phosphatidylcholine and Chol where the phase is uniform.[15,45,46] This difference in phase behavior could stem from the heterogeneity in the lipid precursor mixtures used in each method.[47] In the lipid samples used in the vesicle and bicelle methods, which are vesicles and bicelles, respectively, Chol can be uniformly distributed, and hence, SLBs formed from those precursors have a uniform phase. However, we cannot totally exclude the phase separation because it could be that either the phases are too small to be observed under the microscope or their transition is too continuous (i.e., without first-order change) to be detected.[48,49] On the other hand, the distribution in precursor mixtures for SALB can be nonuniform during a series of phase transitions that take place before SLB formation,[49−51] and therefore, the heterogeneity of the lipid mixtures could likely explain the phase separation observed in the SALB method.

We also compare the Chol enrichment in SLB (Figure 5D). With vesicle fusion, the Chol fraction in SLB is much lower than the input Chol fraction (maximum of 10 mol % Chol in SLB for input Chol of 20 mol %), whereas with SALB, Chol is enriched and exists in domains that increase linearly with input Chol up to 60 mol %. By contrast, the bicelle method also can enrich Chol in complete SLBs formed with up to 30 mol % input Chol. For the cases of incomplete SLB formation with 40−60 mol % Chol, the positive QCM-D Δf shifts during MβCD treatment and approximate Chol estimation (as described above, the Sauerbrey relationship is invalid for these cases, and hence, the Chol content is only estimated; data not shown) suggest Chol is enriched in incomplete SLBs too.

Collectively, the results support that different lipid aggregation properties between the three methods can lead

DOI: 10.1021/acs.langmuir.9b02851
Langmuir 2019, 35, 15063−15070

to different mechanics in SLB formation as well as different SLB properties and Chol enrichment.

CONCLUSIONS

Herein, we demonstrated the SLB formation from cholesterol-rich bicelles. The QCM-D and fluorescence microscopy techniques were used to characterize the formation, morphology, and mobility of supported lipid membranes. The results revealed that complete SLBs are formed with bicelles containing up to 30 mol % Chol and incomplete SLBs from 40 to 60 mol % Chol, and all SLBs are enriched in Chol. By comparison, the vesicle fusion method can form SLBs with up to 20 mol % Chol, but SLBs are not Chol-enriched, whereas the SALB method can form SLBs that are enriched with Chol up to 60 mol %. These differences are likely due to different lipid assembly properties among the methods and need to be considered when choosing the appropriate method for fabricating SLBs. For example, although SALB has high Chol enrichment, the use of organic solvents may pose challenges in some applications such as protein incorporation. In such cases, the bicelle method can be a better option since it is operated in aqueous solution and also capable of Chol enrichment. Altogether, this work has shown the capacity of bicelles to form SLBs with Chol and contributes to finding optimal experimental parameters for the bicelle method.

ASSOCIATED CONTENT

Supporting Information

The Supporting Information is available free of charge on the ACS Publications website at DOI: 10.1021/acs.langmuir.9b02851.

Additional information is provided about fluorescence recovery after photobleaching (FRAP) method, FRAP observation of fluidic cholesterol-enriched supported lipid membranes on silicon dioxide (Figure S1), and cholesterol depletion by methyl-β-cyclodextrin (MβCD) treatment (Figure S2) (PDF)

AUTHOR INFORMATION

Corresponding Author

*Email: njcho@ntu.edu.sg.

ORCID

Soohyun Park: 0000-0003-3261-7585

Nam-Joon Cho: 0000-0002-8692-8955

Notes

The authors declare no competing financial interest.

ACKNOWLEDGMENTS

This work was supported by the Center for Precision Biology at Nanyang Technological University.

REFERENCES

(1) Yeagle, P. L. Cholesterol and the Cell Membrane. *Biochim. Biophys. Acta, Rev. Biomembr.* **1985**, *822*, 267−287.

(2) McMullen, T. P. W.; Lewis, R. N. A. H.; McElhaney, R. N. Cholesterol−Phospholipid Interactions, the Liquid-Ordered Phase and Lipid Rafts in Model and Biological Membranes. *Curr. Opin. Colloid Interface Sci.* **2004**, *8*, 459−468.

(3) Ohvo-Rekilä, H.; Ramstedt, B.; Leppimäki, P.; Slotte, J. P. Cholesterol Interactions with Phospholipids in Membranes. *Prog. Lipid Res.* **2002**, *41*, 66−97.

(4) Rodal, S. K.; Skretting, G.; Garred, Ø.; Vilhardt, F.; Van Deurs, B.; Sandvig, K. Extraction of Cholesterol with Methyl-β-Cyclodextrin Perturbs Formation of Clathrin-Coated Endocytic Vesicles. *Mol. Biol. Cell* **1999**, *10*, 961−974.

(5) Subtil, A.; Gaidarov, I.; Kobylarz, K.; Lampson, M. A.; Keen, J. H.; McGraw, T. E. Acute Cholesterol Depletion Inhibits Clathrin-Coated Pit Budding. *Proc. Natl. Acad. Sci. U. S. A.* **1999**, *96*, 6775−6780.

(6) Qin, C.; Nagao, T.; Grosheva, I.; Maxfield, F. R.; Pierini, L. M. Elevated Plasma Membrane Cholesterol Content Alters Macrophage Signaling and Function. *Arterioscler., Thromb., Vasc. Biol.* **2006**, *26*, 372−378.

(7) Mason, R. P.; Tulenko, T. N.; Jacob, R. F. Direct Evidence for Cholesterol Crystalline Domains in Biological Membranes: Role in Human Pathobiology. *Biochim. Biophys. Acta, Biomembr.* **2003**, *1610*, 198−207.

(8) Hardy, G. J.; Nayak, R.; Zauscher, S. Model Cell Membranes: Techniques to Form Complex Biomimetic Supported Lipid Bilayers via Vesicle Fusion. *Curr. Opin. Colloid Interface Sci.* **2013**, *18*, 448−458.

(9) De Almeida, R. F. M.; Fedorov, A.; Prieto, M. Sphingomyelin/Phosphatidylcholine/Cholesterol Phase Diagram: Boundaries and Composition of Lipid Rafts. *Biophys. J.* **2003**, *85*, 2406−2416.

(10) Veatch, S. L.; Keller, S. L. Miscibility Phase Diagrams of Giant Vesicles Containing Sphingomyelin. *Phys. Rev. Lett.* **2005**, *94*, 148101.

(11) Bacia, K.; Schwille, P.; Kurzchalia, T. Sterol Structure Determines the Separation of Phases and the Curvature of the Liquid-Ordered Phase in Model Membranes. *Proc. Natl. Acad. Sci. U. S. A.* **2005**, *102*, 3272−3277.

(12) Mashaghi, A.; Mashaghi, S.; Reviakine, I.; Heeren, R. M. A.; Sandoghdar, V.; Bonn, M. Label-Free Characterization of Biomembranes: From Structure to Dynamics. *Chem. Soc. Rev.* **2014**, *43*, 887−900.

(13) Richter, R. P.; Bérat, R.; Brisson, A. R. Formation of Solid-Supported Lipid Bilayers: An Integrated View. *Langmuir* **2006**, *22*, 3497−3505.

(14) Jackman, J. A.; Choi, J.-H.; Zhdanov, V. P.; Cho, N.-J. Influence of Osmotic Pressure on Adhesion of Lipid Vesicles to Solid Supports. *Langmuir* **2013**, *29*, 11375−11384.

(15) Sundh, M.; Svedhem, S.; Sutherland, D. S. Influence of Phase Separating Lipids on Supported Lipid Bilayer Formation at Sio 2 Surfaces. *Phys. Chem. Chem. Phys.* **2010**, *12*, 453−460.

(16) Tabaei, S. R.; Jackman, J. A.; Kim, S.-O.; Liedberg, B.; Knoll, W.; Parikh, A. N.; Cho, N.-J. Formation of Cholesterol-Rich Supported Membranes Using Solvent-Assisted Lipid Self-Assembly. *Langmuir* **2014**, *30*, 13345−13352.

(17) Tabaei, S. R.; Jackman, J. A.; Liedberg, B.; Parikh, A. N.; Cho, N.-J. Observation of Stripe Superstructure in the Beta-Two-Phase Coexistence Region of Cholesterol-Phospholipid Mixtures in Supported Membranes. *J. Am. Chem. Soc.* **2014**, *136*, 16962−16965.

(18) Tabaei, S. R.; Jackman, J. A.; Kim, M.; Yorulmaz, S.; Vafaei, S.; Cho, N.-J. Biomembrane Fabrication by the Solvent-Assisted Lipid Bilayer (SALB) Method. *J. Visualized Exp.* **2015**, *106*, No. e53073.

(19) Tabaei, S. R.; Choi, J.-H.; Haw Zan, G.; Zhdanov, V. P.; Cho, N.-J. Solvent-Assisted Lipid Bilayer Formation on Silicon Dioxide and Gold. *Langmuir* **2014**, *30*, 10363−10373.

(20) Tabaei, S. R.; Jackman, J. A.; Kim, S.-O.; Zhdanov, V. P.; Cho, N.-J. Solvent-Assisted Lipid Self-Assembly at Hydrophilic Surfaces: Factors Influencing the Formation of Supported Membranes. *Langmuir* **2015**, *31*, 3125−3134.

(21) Tabaei, S. R.; Vafaei, S.; Cho, N.-J. Fabrication of Charged Membranes by the Solvent-Assisted Lipid Bilayer (SALB) Formation Method on Sio 2 and Al 2 O 3. *Phys. Chem. Chem. Phys.* **2015**, *17*, 11546−11552.

(22) Ram, P.; Prestegard, J. H. Magnetic Field Induced Ordering of Bile Salt/Phospholipid Micelles: New Media for NMR Structural Investigations. *Biochim. Biophys. Acta, Biomembr.* **1988**, *940*, 289−294.

DOI: 10.1021/acs.langmuir.9b02851
Langmuir 2019, 35, 15063−15070

(23) Marcotte, I.; Auger, M. Bicelles as Model Membranes for Solid- and Solution-State NMR Studies of Membrane Peptides and Proteins. *Concepts Magn. Reson., Part A* **2005**, *24A*, 17−37.
(24) van Dam, L.; Karlsson, G.; Edwards, K. Direct Observation and Characterization of DMPC/DHPC Aggregates under Conditions Relevant for Biological Solution NMR. *Biochim. Biophys. Acta, Biomembr.* **2004**, *1664*, 241−256.
(25) Dürr, U. H.; Soong, R.; Ramamoorthy, A. When Detergent Meets Bilayer: Birth and Coming of Age of Lipid Bicelles. *Prog. Nucl. Magn. Reson. Spectrosc.* **2013**, *69*, 1.
(26) Zeineldin, R.; Last, J. A.; Slade, A. L.; Ista, L. K.; Bisong, P.; O'Brien, M. J.; Brueck, S. R. J.; Sasaki, D. Y.; Lopez, G. P. Using Bicellar Mixtures to Form Supported and Suspended Lipid Bilayers on Silicon Chips. *Langmuir* **2006**, *22*, 8163−8168.
(27) Tabaei, S. R.; Jönsson, P.; Brändén, M.; Höök, F. Self-Assembly Formation of Multiple DNA-Tethered Lipid Bilayers. *J. Struct. Biol.* **2009**, *168*, 200−206.
(28) Morigaki, K.; Kimura, S.; Okada, K.; Kawasaki, T.; Kawasaki, K. Formation of Substrate-Supported Membranes from Mixtures of Long-and Short-Chain Phospholipids. *Langmuir* **2012**, *28*, 9649−9655.
(29) Kolahdouzan, K.; Jackman, J. A.; Yoon, B. K.; Kim, M. C.; Johal, M. S.; Cho, N.-J. Optimizing the Formation of Supported Lipid Bilayers from Bicellar Mixtures. *Langmuir* **2017**, *33*, 5052−5064.
(30) Sut, T. N.; Jackman, J. A.; Yoon, B. K.; Park, S.; Kolahdouzan, K.; Ma, G. J.; Zhdanov, V. P.; Cho, N.-J. Influence of NaCl Concentration on Bicelle-Mediated SLB Formation. *Langmuir* **2019**, *35*, 10658−10666.
(31) Sut, T. N.; Jackman, J. A.; Cho, N.-J. Understanding How Membrane Surface Charge Influences Lipid Bicelle Adsorption onto Oxide Surfaces. *Langmuir* **2019**, *35*, 8436−8444.
(32) Cho, N.-J.; Frank, C. W.; Kasemo, B.; Höök, F. Quartz Crystal Microbalance with Dissipation Monitoring of Supported Lipid Bilayers on Various Substrates. *Nat. Protoc.* **2010**, *5*, 1096.
(33) Keller, C.; Kasemo, B. Surface Specific Kinetics of Lipid Vesicle Adsorption Measured with a Quartz Crystal Microbalance. *Biophys. J.* **1998**, *75*, 1397−1402.
(34) Maxfield, F. R.; Tabas, I. Role of Cholesterol and Lipid Organization in Disease. *Nature* **2005**, *438*, 612.
(35) Huang, J.; Buboltz, J. T.; Feigenson, G. W. Maximum Solubility of Cholesterol in Phosphatidylcholine and Phosphatidylethanolamine Bilayers. *Biochim. Biophys. Acta, Biomembr.* **1999**, *1417*, 89−100.
(36) Mainali, L.; Raguz, M.; Subczynski, W. K. Formation of Cholesterol Bilayer Domains Precedes Formation of Cholesterol Crystals in Cholesterol/Dimyristoylphosphatidylcholine Membranes: Epr and Dsc Studies. *J. Phys. Chem. B* **2013**, *117*, 8994−9003.
(37) Gaemers, S.; Bax, A. Morphology of Three Lyotropic Liquid Crystalline Biological NMR Media Studied by Translational Diffusion Anisotropy. *J. Am. Chem. Soc.* **2001**, *123*, 12343−12352.
(38) Triba, M. N.; Devaux, P. F.; Warschawski, D. E. Effects of Lipid Chain Length and Unsaturation on Bicelles Stability. A Phosphorus NMR Study. *Biophys. J.* **2006**, *91*, 1357−1367.
(39) Nieh, M.-P.; Raghunathan, V. A.; Glinka, C. J.; Harroun, T. A.; Pabst, G.; Katsaras, J. Magnetically Alignable Phase of Phospholipid "Bicelle" Mixtures Is a Chiral Nematic Made up of Wormlike Micelles. *Langmuir* **2004**, *20*, 7893−7897.
(40) Rodríguez, G.; Cócera, M.; Rubio, L.; López-Iglesias, C.; Pons, R.; de la Maza, A.; López, O. A Unique Bicellar Nanosystem Combining Two Effects on Stratum Corneum Lipids. *Mol. Pharmaceutics* **2012**, *9*, 482−491.
(41) Carnell, M.; Macmillan, A.; Whan, R. Fluorescence Recovery after Photobleaching (Frap): Acquisition, Analysis, and Applications. *Methods Membr. Lipids* **2015**, 255−271.
(42) Beseničar, M. P.; Bavdek, A.; Kladnik, A.; Maček, P.; Anderluh, G. Kinetics of Cholesterol Extraction from Lipid Membranes by Methyl-β-Cyclodextrin—a Surface Plasmon Resonance Approach. *Biochim. Biophys. Acta, Bioenerg.* **2008**, *1778*, 175−184.
(43) Sauerbrey, G. Z. Use of Quartz Crystal Units for Weighing Thin Films and Microweighing. *Magzine for Physics* **1959**, *155*, 206−222.
(44) Ferhan, A. R.; Yoon, B. K.; Park, S.; Sut, T. N.; Chin, H.; Park, J. H.; Jackman, J. A.; Cho, N.-J. Solvent-Assisted Preparation of Supported Lipid Bilayers. *Nat. Protoc.* **2019**, *14*, 2091.
(45) Veatch, S. L.; Keller, S. L. Seeing Spots: Complex Phase Behavior in Simple Membranes. *Biochim. Biophys. Acta, Mol. Cell Res.* **2005**, *1746*, 172−185.
(46) Zhao, J.; Wu, J.; Heberle, F. A.; Mills, T. T.; Klawitter, P.; Huang, G.; Costanza, G.; Feigenson, G. W. Phase Studies of Model Biomembranes: Complex Behavior of DSPC/DOPC/Cholesterol. *Biochim. Biophys. Acta, Biomembr.* **2007**, *1768*, 2764−2776.
(47) Crane, J. M.; Tamm, L. K. Role of Cholesterol in the Formation and Nature of Lipid Rafts in Planar and Spherical Model Membranes. *Biophys. J.* **2004**, *86*, 2965−2979.
(48) Nicolini, C.; Thiyagarajan, P.; Winter, R. Small-Scale Composition Fluctuations and Microdomain Formation in Lipid Raft Models as Revealed by Small-Angle Neutron Scattering. *Phys. Chem. Chem. Phys.* **2004**, *6*, 5531−5534.
(49) Feigenson, G. W. Phase Diagrams and Lipid Domains in Multicomponent Lipid Bilayer Mixtures. *Biochim. Biophys. Acta, Biomembr.* **2009**, *1788*, 47−52.
(50) Hohner, A. O.; David, M. P. C.; Rädler, J. O. Controlled Solvent-Exchange Deposition of Phospholipid Membranes onto Solid Surfaces. *Biointerphases* **2010**, *5*, 1−8.
(51) Szoka, F.; Papahadjopoulos, D. Procedure for Preparation of Liposomes with Large Internal Aqueous Space and High Capture by Reverse-Phase Evaporation. *Proc. Natl. Acad. Sci.* **1978**, *75*, 4194−4198.

DOI: 10.1021/acs.langmuir.9b02851
Langmuir 2019, 35, 15063−15070